Berenguer Betrián, R.; Quijada, C.; Morallón, E. (2019). The nature of the electro-catalytic response of mixed metal oxides: Pt- and Ru-doped SnO2 anodes. ChemElectroChem. 6(4):1057-1068. https://doi.org/10.1002/celc.201801632

FUNDAMENTALS & APPLICATIONS

CHEMELECTROCHEM

ANALYSIS & CATALYSIS, BIO & NANO, ENERGY & MORE

Accepted Article

Title: On the nature of the electro-oxidative catalytic response of mixed metal oxides: the case of Pt- and Ru-doped SnO2 anodes

Authors: R. Berenguer, C. Quijada, and Emilia Morallon

To be cited as: *ChemElectroChem* 10.1002/celc.201801632

Link to VoR: http://dx.doi.org/10.1002/celc.201801632

A Journal of

ChemPubSoc Europe

WILEY-VCH

www.chemelectrochem.org

On the nature of the electro-oxidative catalytic response of mixed metal oxides: the case of Pt- and Ru-doped SnO_2 anodes

R. Berenguer[a], C. Quijada[b] and E. Morallón[a]

[a]Departamento de Química Física e Instituto Universitario de Materiales. Universidad de Alicante. Apartado 99. E-03080 Alicante (Spain)

[b] Departamento de Ingeniería Textil y Papelera, Universitat Politècnica de València. Pza Ferrándiz y Carbonell, E-03801 Alcoy (Alicante). Spain

Abstract

The catalytic behavior of metal oxides for oxidative reactions is generally classified into active or non-active depending on whether surface redox species participate or not. In the case of mixed metal oxides, however, this simplified scenario may be more complex. Non-active oxides containing electroactive metal species (Pt- and/or Ru), are promising anodes for the electrochemical treatment of wastewaters. This work analyzes the effect of Pt and Ru species on the nature of the electro-oxidative catalytic response of Ti/SnO_2 anodes. For this purpose, the electro-oxidation of phenol and the competing oxygen evolution reaction (OER) in NaOH have been studied. The different electrodes and reactions were characterized by cyclic voltammetry, electrochemical impedance spectroscopy, and Tafel measurements. The obtained results reveal that both Pt and Ru introduce solid-state redox processes and catalyze the OER and the phenol oxidation onto Ti/SnO_2-based electrodes. Nevertheless, the dopants induce different active behaviors in the mixed oxides. Pt practically does not affect the OER mechanism, but enhances its kinetics, so its electrocatalytic activity is associated with a specific adsorption of hydroxyl anions or phenolate, without participation of the irreversible Pt/PtOx couple. On the contrary, Ru species involve various and highly reversible redox processes that accelerate and modify the rate-determining step of the OER, and that actively mediate in the phenol oxidation.

Corresponding author:
E. Morallón
morallon@ua.es

1. Introduction

The application of electrochemistry in environmental issues, such as the abatement of pollutants for wastewater treatment, has received great interest due to various advantages, namely, it is cheap, environmentally clean and simple to handle and control [1-3]. Nevertheless, the real feasibility of the electrochemical technology for this application relies on the right choice of a suitable anode. In this sense, apart from good electrocatalytic properties, a high stability and a low price are essential.

A vast literature is available on the anodic oxidation of pollutants on different anodes. In principle, three different anodic processes have been proposed [4]. First, at high anodic potentials, in the region of water discharge, oxidation of pollutants is mediated by the same surface intermediates of the oxygen evolution reaction (OER), i.e. through adsorbed hydroxyl radicals (•OH). The occurrence of these competitive surface reactions was first rationalized by Comninellis et al. [5]. According to this model, the electro-oxidative behavior of anodes can be *active*, through chemisorbed radicals favoring a more selective oxidation; or *non-active*, via physisorbed radicals promoting the non-selective oxidation and mineralization of organics. Second, the oxidation of pollutants can occur indirectly in the solution via strongly oxidant species that are electrogenerated in-situ on the anode at high potentials [2,6]. Finally, Scialdone et al. proposed that the direct electrochemical oxidation of the pollutant may proceed at lower potentials (prior the OER) on the surface of different types of anodes [7-9].

The formation and reactivity of hydroxyl radicals was studied by different authors [5, 10-13]. Kapalka et al. demonstrated that the formation of quasi free •OH on *non-active* boron doped diamond (BDD) electrode is a fast reaction [12], showing higher oxidizing power than those formed on other anodes [11,13]. In consequence, BDD is generally considered the most effective anode for the oxidation and/or mineralization organic pollutants [14,15]. On the other hand, pure (MOx) and mixed (M'MOx) metal oxides, generally deposited on Ti (the so-called dimensionally stable anodes, DSAs), exhibit matchless versatility and lower price than expensive metal and BDD electrodes [16,17]. Therefore, they are considered excellent alternative anodes for the electrochemical oxidation of biorefractory organic pollutants in wastewaters [5,18]. So far, several MOx and M'MOx have been extensively studied in the past, and doping metal oxides with stabilizing and/or electroactive/catalytic species is one of the most studied subjects in this research field. In general, the higher the overpotential for the OER on the anode material (*non-*

active character), the weaker its interaction with •OHs and the higher their effectivity toward organics oxidation.

The model proposed by Comninellis is, then, quite useful to explain the different oxidizing capability of a wide variety of anode materials in a simple way. The model has been successfully applied to predict the kinetics of organics oxidation in the case of BDD [11,19-21] and, with a lower degree of accuracy, on certain *active* anodes, like IrO_2–Ta_2O_5 [8,9] or RuO_2 [22]. Despite it is still generally accepted, the model has been validated to represent only the two limiting behaviors for which it was proposed 24 years ago [5], i.e. the oxidation response of *non-active* and *active* anodes. In this context, the following questions arise: (i) is there something new on the electrochemical behavior of mixed metal oxides? (ii) how do behave mixed-metal oxides containing species of different nature: *active* + *non-active*? At least, the authoritative reviews on the field neither answer nor mention these questions [2-4,23-26].

It is well known that both *primary* and *secondary* electrocatalytic effects can be distinguished in these mixed metal oxides. The first one involves a direct effect of composition and nature of the active component on the reaction activation energy; and the latter is related to the diverse structure (accessibility, morphology, specific area, etc.) of the electrode surface [17,27]. In this sense, understanding and discerning *primary* (true) from *secondary* (geometric) electrocatalytic factors is crucial for the design of new improved M'MOs anodes.

Among the wide variety of metal oxides, Sb-doped SnO_2 anodes gather low cost and high overvoltage for the oxygen evolution reaction (OER), this latter feature being remarkable for the electrochemical combustion of organic pollutants from aqueous wastes [28-32]. The Sb dopant (13 at. % in this work) merely increases the low conductivity of SnO_2. However, these oxides show low electrochemical stability under anodic polarization [33-36], what may restrict their application.

Different approaches have been proposed to increase the stability of the SnO_2-based electrodes, but most of them were tested in acid electrolytes [34-36]. In this medium, the effect of the Pt loading (0, 3, or 13 at. %) on the stability [36] and phenol electro-oxidation activity [32] of Ti/SnO_2-Sb was studied. Interestingly, it was found that the electrode with a 3 at. % Pt shows the best performance in both stability and oxidation efficiency. The worse performance of the anode with 13 at% Pt was reasonably justified by the much stronger competition with the OER on this anode. However, the unexpected better performance of the 3 at. % Pt electrode, compared to that

without Pt, was justified by the higher compactness level of this electrode, i.e. in terms of geometric factors [32].

On the other hand, the study of stability and deactivation mechanisms of new DSA electrodes in alkaline conditions has received much less attention [37-39]. We have studied the influence of Ru loading (0 - 13.00 at. % Ru), by replacing Sb, on the response of the Ti/SnO_2-Sb electrodes with a fixed 3 at. % Pt (Ti/SnO_2–Sb(13−x)–Ru(x)–Pt(3) electrodes). We found that the stability (service life) of Sb-doped Ti/SnO_2 anodes in alkaline medium increases significantly by the incorporation of a small amount (ca. 3 at. %) of either Pt or both Pt and Ru [39]. In addition, we have recently demonstrated that, considering all relevant criteria (current efficiency, energy consumption, stability and cost), the performance of this Pt- and Ru-doped Ti/SnO_2-Sb electrode for the electrochemical treatment of alkaline phenolic wastewaters is remarkably superior to that of conventional Ti/RuO_2 and Ti/Co_3O_4 anodes [40]. This was related to electronic factors. Nevertheless, in this previous study the influence of Pt was not separately analyzed from that of Ru. Moreover, under electrolytic conditions, both the phenol electro-oxidation and the OER proceed together, so that, the occurrence of a single or various reaction could also influence the determining electrocatalytic factors [32,41]. Thus, the different metals and/or the different electrolyte and electrochemical conditions (acid vs. basic medium; one vs. various reactions) resulted in a different, conflicting, catalytic behavior, governed by geometric or electronic factors.

It can be then inferred that, despite their interesting properties, the factors determining the electrocatalytic response of Pt- and Ru-doped SnO_2-based anodes are still uncertain. Moreover, the influence of these electroactive species on the *non-active* nature of SnO_2 has not been either investigated or rationalized yet. To tackle these two important issues, the specific role and influence of each dopant, Pt or Ru, on the response of SnO_2 anodes should be investigated separately on each reaction involved. In this work, the effect of Pt or Ru on the electrocatalytic behavior of Ti/SnO_2-Sb anodes has been studied for the OER and the electro-oxidation of phenol under alkaline conditions. For such a purpose, three different Ti/SnO_2-based electrodes, with nominal compositions Ti/SnO_2-Sb(13%), Ti/SnO_2-Sb(13%)-Pt(3%) and Ti/SnO_2-Ru(13%), and (for comparison) a Ti/RuO_2 electrode, have been prepared by the conventional thermal decomposition technique. The morphology and composition of the electrodes were characterized by scanning electron microscopy coupled to energy-dispersive X-Ray microanalysis (SEM-EDX). The surface-related *secondary* electrocatalytic effects were analyzed by cyclic

voltammetry (CV) and electrochemical impedance spectroscopy (EIS). The mechanism and *primary* electrocatalytic activity towards both reactions were investigated by CV, Tafel plots and EIS.

2. Experimental

2.1. Preparation of the electrodes

The metal oxide electrodes chosen for this study were Ti/SnO_2-Sb(13%), Ti/SnO_2-Sb(13%)-Pt(3%), Ti/SnO_2-Ru(13%) and Ti/RuO_2 (the percentage in brackets indicating the metal atomic composition). These oxides were prepared as thin films by thermal decomposition of proper salt precursors ($SnCl_4$*x*$5H_2O$, $SbCl_3$, H_2PtCl_6 and $RuCl_3$*x*nH_2O, in acidified absolute ethanol) onto a Ti sheet support (1 cm x 1cm), as reported elsewhere [39,40,42]. As explained in the introduction section, the electrode with a 3 at. % Pt has been chosen for this study because it showed the best performance (stability and activity) and because of its controversial catalytic behavior. In the case of Ru, the electrode with 13 at. % Ru, without Sb, has been used because Ru itself enhances the conductivity of SnO_2. Since no quantitative comparisons are made, the different metal loadings are not expected to affect the qualitative study presented in this work. Both Ti/SnO_2-Sb and Ti/RuO_2 are used for the sake of comparison.

Then, whenever the text is referred to an electrode (coating and support), Ti/XXX nomenclature has been used. Nevertheless, whenever the text is exclusively referred to an inherent property of the coating or SnO_2-based oxides (independently on whether it is supported on Ti or not), then, it is indicated by the absence of "Ti/".

2.2. Characterization of the electrodes

The morphology and composition of the oxides was studied by scanning electron microscopy (SEM) in a Hitachi S-3000N microscope coupled to energy-dispersive X-ray (EDX) spectroscopy with a Rontec X-ray detector. The electrochemical behavior of the electrodes was studied by cyclic voltammetry (CV), electrochemical impedance spectroscopy (EIS) and Tafel measurements in a conventional three electrode cell (see a scheme of the electrochemical set-up in the supporting information (SI)). The counter electrode was a Pt wire electrode and the potentials are referred to a reversible hydrogen electrode (RHE) immersed in the same electrolyte solution. The aqueous 0.1 M NaOH electrolyte solutions were de-

oxygenated by N_2 bubbling and were prepared from Merck p.a. reagent and ultrapure water (Purelab Ultra from Elga-Vivendi, 18.2MΩ cm).

For the calculation of the double-layer capacitance and voltammetric charges of the electrodes, several voltammetric measurements were performed between different potential limits at various scan rates, between 1 mV s^{-1} and 5000 mV s^{-1}. Then, these parameters were determined by conventional methods [43] (more detail on these methods can be found in the main text and the SI). The current densities were calculated by using the apparent geometric area of the electrodes (2 cm^2). For the study of phenol electro-oxidation, at 1000 ppm phenol (Merck p.a.) + 0.1 M NaOH aqueous solution was prepared. This high concentration of phenol was chosen because it represents a more real scenario of wastewater that can be feasibly treated by anodic oxidation [25]. Besides, the influence of the phenol concentration (200-1000 ppm) was analyzed.

The electrocatalytic activity towards OER was investigated by Tafel measurements [43]. The quasi-steady galvanostatic curves were obtained at current densities lower than 5 mA cm^{-2} at a scan rate of 3 μA s^{-1}. Both CV and Tafel analysis were carried out by using an Autolab PGSTAT 30 system.

EIS was performed at room temperature, in a constant voltage mode (1.0 V - 1.8 V vs RHE), by sweeping frequencies from 100 kHz to 10 mHz at an amplitude of 5 mV. These analyses were carried out on a FRD-100 Frequency Response Detector module connected to the EG&G model 273 potentionstat/galvanostat. The measured EIS data were analyzed and fitted by using ZView® software.

3. Results and Discussion

3.1. SEM and EDX characterization

The obtained electrodes display a cracked-mud structure (Fig. S1), which is characteristic of metal oxide coatings prepared by thermal decomposition [16,33-40,42]. Particularly, the Ti/RuO_2 electrode presents a remarkably lower number of cracks and larger plates than the Ti/SnO_2-based electrodes. When Pt or Ru is introduced on the Ti/SnO_2-Sb electrode, the coatings become less cracked and porous. This compacting effect caused by Pt or Ru has been previously observed and seems to agree with the much higher stability of these doped electrodes in alkaline medium [39]. On the other hand, EDX microanalysis (x500 magnification) evidenced a uniform

distribution of the components and a negligible signal from the underlying Ti support (< 1 %), reflecting a good coverage of the substrate. According to the methodology reported elsewhere [36,42], the coating thickness estimated from the oxide loadings ranged between 2 μm and 3 μm.

The composition and crystalline structure of these electrodes have been described in previous papers [38,39]. Among their properties, it is stressed that Ru replaces the Sn(IV) cations to form a homogeneous $(Ru_{\delta}Sn_{1-\delta})O_2$ single-phase, whereas Pt is not incorporated into the rutile crystalline structure of SnO_2. Above 9.75 at. % some Ru starts to segregate as RuO_2 [39], but Pt is uniformly distributed throughout all the SnO_2 coating in the form of small aggregates with different oxidation states (0, II and, mainly, IV) [39,44]. XRD patterns and EXAFs spectra revealed the presence of metallic platinum dispersed in the oxide layer of Ti/SnO_2-Sb-Pt [45], although it was practically undiscernible at the lowest loadings [39]. The metallic Pt crystallite size increased between 60-100 Å with the amount of platinum (from 3 to 13 at. %). Other platinum phases were not observed by XRD, in agreement with other Pt-doped SnO_2 materials [46]. It is noteworthy to mention that this type of electrodes, in which Pt is embedded in the SnO_2 matrix during thermal decomposition of the mixed precursors, are totally different to those on which metallic Pt particles are deposited on a SnO_2/SnO_2-Sb material [47]. Considering the low relative intensity of metallic Pt diffraction peaks in the studied electrodes, at least in the case of 3 at. % Pt [39], most platinum may be in the form of amorphous PtOx phases. The dimensions of these Pt-enriched phases dispersed in the Ti/SnO_2-Sb-Pt electrodes have not been measured yet. We have roughly estimated the size of these phases from EDX mapping of a Ti/SnO_2-Sb-Pt(3%) electrode. As it can be observed in Figure 1, the Pt-enriched phases are uniformly distributed through the coating and may be below 1 μm, between 200-500 nm in most cases. These dimensions could be important for the electrocatalytic behavior of this electrode, as discussed below (see section 3.5.1).

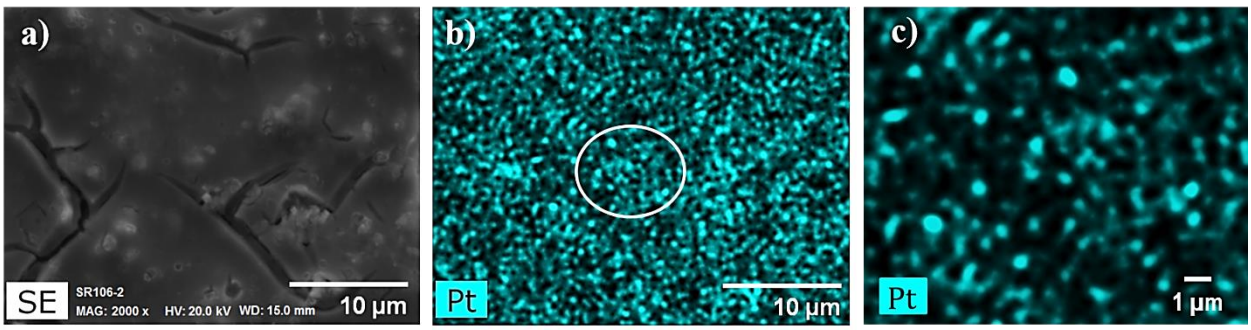

Figure 1. SEM-EDX mapping images of a Ti/SnO_2-Sb-Pt electrode: a) secondary-electrons image; b) Pt-EDX mapping of a); c) magnification of circled region in b).

3.2. General electrochemical behavior of the electrodes

Figure 2 shows the voltammograms of the different electrodes in a 0.1 M NaOH solution. The lack of any voltammetric feature in the profile of the Ti/SnO_2-Sb electrode (Fig. 2A) suggests that the recorded current must be purely capacitive. On the other hand, the anodic current considerably rises above 1.8 V due to the OER. The onset potential for the OER is considerably high when compared to other materials, like noble metals, Co_3O_4, IrO_2, etc. [16,48]. When this anode is doped with Pt, two broad and irreversible electrochemical processes (A_1/C_1) are discernable; and the OER shifts ca. 0.2 V towards less positive values. This A_1/C_1 redox couple has been associated to the formation and reduction of platinum oxides (PtOx), respectively [36,39,42].

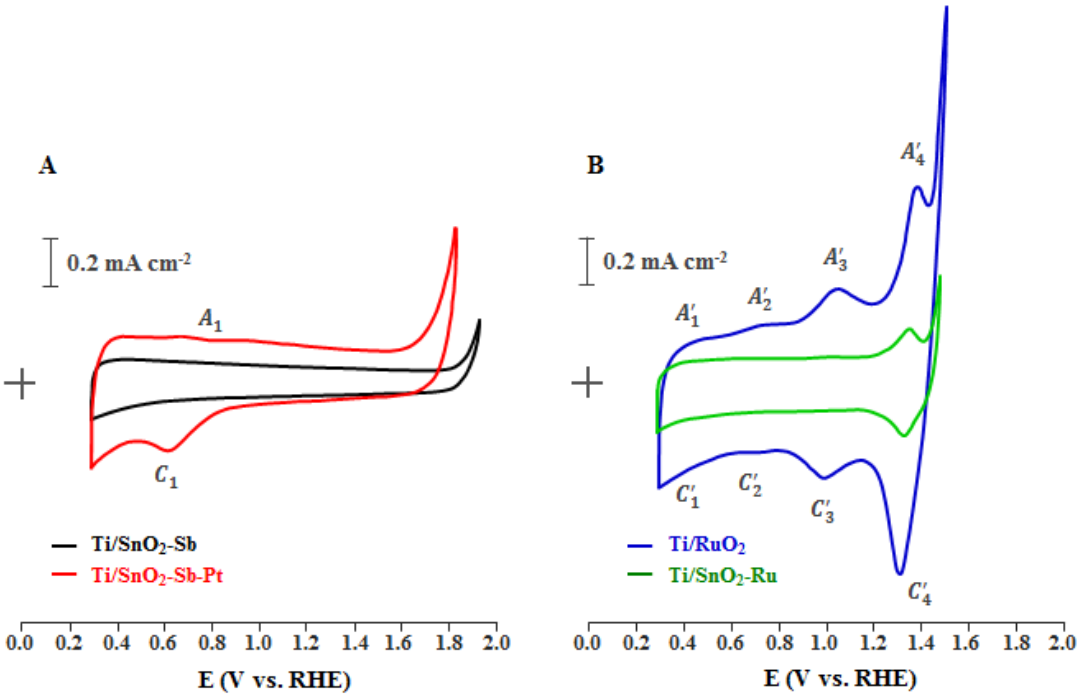

Figure 2. Stabilized cyclic voltammograms of the different electrodes showing the influence of Pt and Ru dopants. Electrolyte = 0.1 M NaOH solution. v = 20 mV s^{-1}.

The voltammogram for the Ti/RuO_2 electrode (Figure 2B) shows clearly diverse redox processes in both the anodic and cathodic scans. These highly reversible surface redox processes are characteristic of this electrode in alkaline medium and have been attributed to Ru(II)↔Ru(III) (A'_1/C'_1); Ru(III)↔Ru(IV) (A'_2/C'_2); Ru(IV)↔Ru(VI) (A'_3/C'_3); and the generation and reduction of higher oxidized oxyruthenium species like Ru(VII) and/or Ru(VIII) (A'_4/C'_4) [49,50]. The sharp current rise occurring at potentials above the A'_4 peak corresponds

to the OER and appears around 0.4 V below than in the case of the Ti/SnO_2-Sb electrode (Fig. 2A).

When the *non-active* Sb is substituted by Ru into the tin oxide (Figure 2B), the OER remarkably shifts towards lower positive potentials, very close to those of the Ti/RuO_2 electrode, and the most prominent A'_4/C'_4 voltammetric peak, related to Ru species, can be clearly observed. Thus, the voltammetric profile of the Ti/SnO_2-Ru electrode in NaOH greatly approaches to that of *active* RuO_2. This is in line with the results of Gaudet et al. [51], who remarked that the shape of the voltammetric curves with a Ru surface content > 28 at. % is similar to that of pure RuO_2.

The electrodes were also characterized by EIS. Nyquist complex-plane plots can be divided into two main regions, namely, the high-frequency (HF) and low-frequency (LF) regions, separated by a transition zone of medium frequencies (MF) (see the whole frequency range in the SI, Fig. S4). Figure 3A displays the HF-Nyquist plots of the studied electrodes registered at 1.2, 1.3 and 1.4 V. Independently of the applied potential, the HF-spectra of the different electrodes (at ca. 100 kHz - 0.1 kHz) are characterized by a depressed semicircle. This semicircle is related to the impedance of the fastest processes occurring at the electrode/solution interface, such as the adsorption of ions and the capacitive behavior [52]. However, this HF region could be also governed by a thin inner TiOx interlayer (around 13 μm [53]) formed at the Ti/MO_2 interface during their thermal preparation treatment. All the electrodes showed analogous semicircles at high frequency, regardless of the applied dc potential. This points out that the resistance associated with this semicircle is similar in all electrodes.

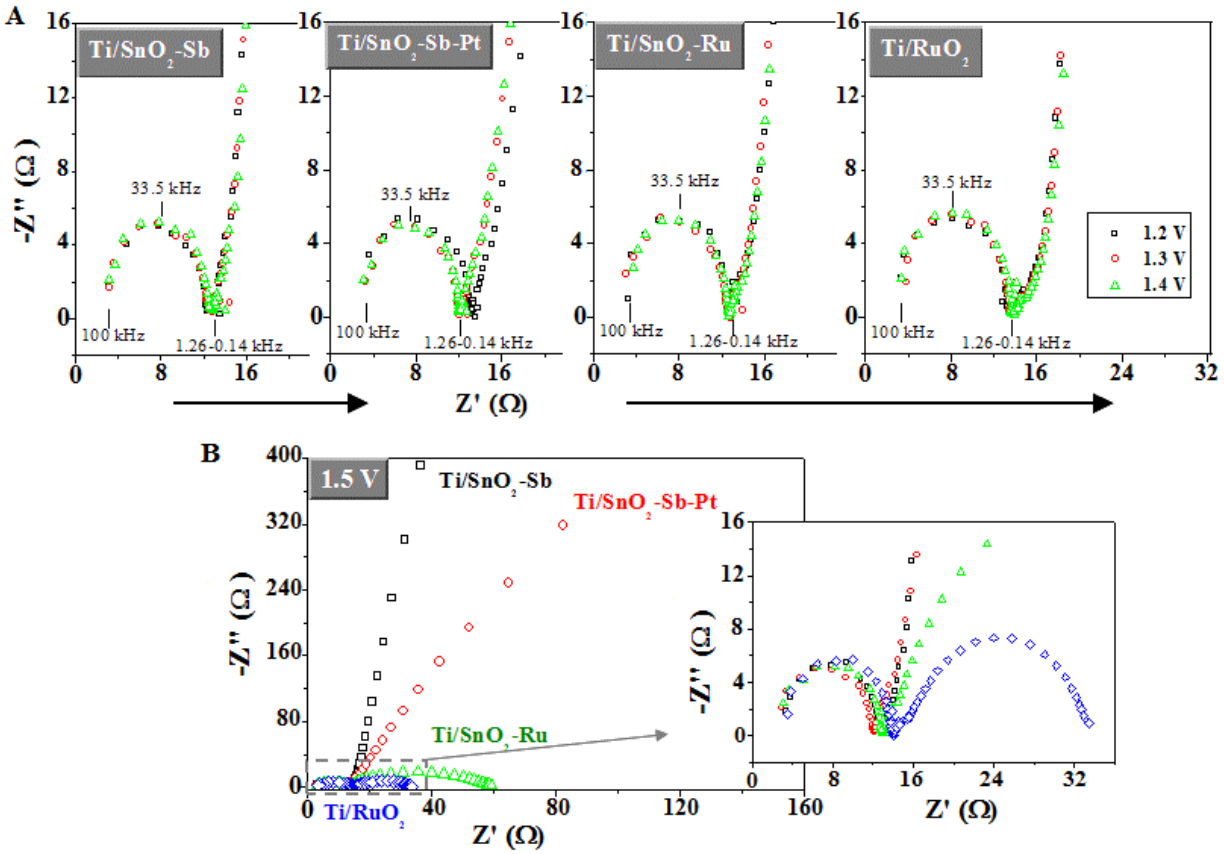

Figure 3. A. The high-frequency Nyquist complex-plane impedance plots for the different electrodes in a 0.1 M NaOH solution at 1.2 V (black squares); 1.3 V (red circles); and 1.4 V (green triangles); B. Magnification of the high-frequency region in Nyquist plots of the different electrodes at 1.5 V.

As the frequency decreases the semicircle completely develops and then, the impedance increases due to time-consuming redox processes [52]. These phenomena involve kinetic or diffusion limitations, i.e. a potential-dependent faradic process, such as adsorption or desorption of electroactive species or a redox reaction. The LF response can adopt two different limiting shapes depending on both the electrode potential and the nature of the electrode: (i) at lower potentials (below 1.4 V), the impedance of most electrodes continuously increases (with the frequency decrease) almost parallel to the imaginary axis (Z¨) (Figure 4A); whereas, (ii) over a given potential, which remarkably depends on the type of electrode, the increasing impedance starts to bend gradually, forming a loop or a developed new semicircle associated to the OER, i.e. a continuous Faradaic reaction. For example, at 1.5 V (Figure 3B) the LF spectrum of Ti/SnO_2-Sb electrode keeps almost vertical, that of Ti/SnO_2-Sb-Pt starts to bend, while those of Ti/SnO_2-Ru and Ti/RuO_2 electrodes completely bend into new semicircles. Thus, Pt or Ru

doping shifts the LF vertical-to-bent transition to lower potentials, reflecting a higher activity towards the OER. These results agree with the voltammetric response.

3.3. Primary and secondary electrocatalytic factors

The electrochemical response of any electrode material towards a given reaction relies on its composition (primary electrocatalytic effects) and surface area (secondary electrocatalytic effects). The available surface area of the electrode exposed to the electrolyte (the so-called *real surface area*, expressed as *a roughness factor (Rf)*) can be estimated from the value of its double-layer capacitance (C_{DL}). The electrochemically-active surface area (the so-called *electrochemical surface area (ECSA)*) is related to the amount, distribution and specific electroactivity of the active sites, and can be determined from the analysis of voltammetric charges (q). The first parameter exclusively depends on geometric factors (secondary effects), whereas the second one also relies on the chemical composition of the oxide layers (primary factors), involving both geometric and electronic effects.

The C_{DL} of the different electrodes was determined by (i) the voltammetric (CV) method and (ii) from EIS measurements. The first method is based on the linear relationship between current density and scan rate [42], and the capacitance is obtained from the slope of these linear plots (see Fig. S3 in SI). The second method takes into account the semicircle-like response of the electrodes at HF in the impedance spectra (Figure 3A) to interpret the capacitive behavior. These semicircles can be fitted by the simple circuit $R_S(C_{DL}R_F)$ (for a complete explanation of the equivalent circuit, see SI), where R_S and R_F are the ohmic resistances associated with the internal elements (electrolyte solution, electrode material, connectors, etc.) and the Faradaic charge transfer through the non-ideally polarizable electrode/solution interface, respectively [52,53]. Table 1 shows the values of C_{DL} of the different electrodes obtained by both techniques at different potentials. In general terms, the values of C_{DL} calculated by EIS are in the order (although slightly lower) of those obtained by CV and follow the same trends. On the one hand, the C_{DL} of the Ti/SnO_2-Sb and Ti/SnO_2-Sb-Pt electrodes decreases with the electrode potential, whereas those of the Ti/SnO_2-Ru and Ti/RuO_2 electrodes increases with this parameter. These behaviors have been attributed to n-type or p-type semiconductors, respectively [36,39]. Nevertheless, in the case of RuO_2, a metallic conductor [54], this evolution of the capacity with the potential has been assigned to structural defects rather than a p-type semiconductor character [55].

Table 1. Specific double-layer capacitance (C_{DL}) and roughness factor (R_f) at various potentials, and electrochemical surface area (*ECSA*), total (q_{TOT}), outer (q_{OUT}) and inner (q_{IN}) voltammetric charges for the different electrodes obtained from the cyclic voltammetric measurements in a 0.1 M NaOH solution.

		Potential V vs. RHE	Electrode			
			Ti/SnO_2-Sb	Ti/SnO_2-Sb-Pt	Ti/SnO_2-Ru	Ti/RuO_2
C_{DL} (mF cm^{-2})	CV	0.55	3.1	3.7	3.4	6.8
		0.75	2.6	3.4	3.5	7.5
		0.95	2.4	3.0	3.5	8.5
	EIS	1.10	0.8	1.4	1.9	2.8
		1.30	0.4	1.3	2.8	3.3
Rf		0.55	389	464	456	85
		0.95	301	376	469	106
ECSA (m^2 g^{-1})			22	70	42	10
Charge (mC cm^{-2})		q_{TOT}	2.87	8.91	5.56	14.98
		q_{OUT}	2.62	5.87	5.00	12.10
		q_{IN}	0.25	3.04	0.56	2.88

On the other hand, for a given potential, the capacitance of the Ti/SnO_2-Sb electrode slightly increases when Pt or Ru is introduced, but it remains lower than in the case of the Ti/RuO_2 electrode. Another suitable parameter for comparison purposes may be the roughness factor (R_f), since it accounts for the specific capacitance of the different materials. Defined as the real to geometric surface area of electrode, the R_f values (Table 1) were calculated by dividing the experimental C_{DL} values by the theoretical specific areal capacitance (C_{AREAL}) of SnO_2-based (8 μF cm^{-2}) [56] and RuO_2 (80 μF cm^{-2}) [57] electrodes. The R_f values for the Ti/SnO_2-based electrodes remarkably increase with Pt and Ru doping and are considerably higher than those of the Ti/RuO_2 electrode. These results point out that the Ti/SnO_2-based electrodes are all much more porous than the Ti/RuO_2 electrode. This finding roughly agrees with SEM images (Figure S1). Thus, the lower surface area (roughness) of the Ti/RuO_2 electrode is well compensated by its higher specific capacitance, finally displaying even higher C_{DL} values.

The total (q_{TOT}), outer (q_{OUT}) and inner (q_{IN}) voltammetric charges of the electrodes were determined as a function of the scan rate according to the voltammetric method developed by Trasatti et al. [58] (see more details in the SI). These charges are related to the total, the most accessible and the less accessible (pores, cracks, grain boundaries, etc.) electroactive surface,

respectively [51]. The *ECSA* (m^2/g) can be calculated from the gravimetric capacitance (F g^{-1}) as proposed in the equation (1)

$$ECSA = \frac{gravimetric\ capacitance}{theoretical\ areal\ capacitance} = \frac{\frac{q_{TOT}}{\Delta V \cdot W_{MOx}}}{C_{AREAL}} \qquad (1)$$

where q_{TOT} is the total charge (Table 1) expressed in C cm^{-2}; ΔV is the voltage window used to calculate the q_{TOT} (0.9-1.0 V); W_{MOx} is the averaged mass loading of the Ti-coated electrodes ($1.60\text{-}1.85 \cdot 10^{-3}$ g cm^{-2}) and C_{AREAL} is the mentioned theoretical specific areal capacitance of SnO_2-based and RuO_2 materials expressed in F m^{-2}. Table 1 collects the calculated values of q_{TOT}, q_{OUT}, q_{IN} and *ECSA* for the different electrodes. The calculated *ECSA* values, ranging between 10-70 m^2/g, follow the same trend as that of *Rf*. Please note that the use of the SnO_2 theoretical specific capacitance (8 μF cm^{-2}), which does not consider the effect of active species, for Pt- and Ru-doped SnO_2 electrodes may lead to slightly overestimated *Rf* and *ECSA* values for these electrodes.

The charge values obtained for the Ti/RuO_2 electrode are much higher than those of the Ti/SnO_2-based electrodes, highlighting the high electroactivity of ruthenium species in alkaline medium. In addition, it should be stressed the relatively high charge shown by the Pt-doped Ti/SnO_2-Sb electrode, which only contains a 3 % of active metal (Pt), compared to that of the Ti/SnO_2-Ru(13%) electrode. This could indicate that not all the Ru introduced in the tin oxide is electrochemically active. These trends do not agree with the observed differences on geometric factors, indicating that the electronic factors related to the electrode composition constitute the key contributions to the voltammetric charges (the electrochemical response) of the studied electrodes.

3.4. Oxygen evolution reaction

The electrochemical activity of the electrodes towards the OER in alkaline medium has been studied by different techniques. First, the voltammetric characterization (Fig. 2) has shown that the introduction of Pt or the replacement of Sb by Ru in the Ti/SnO_2-Sb anode decrease the onset potential for the OER by around 0.2 V and 0.4 V, respectively. In addition, the vertical-to-bent transition of LF impedance spectrum occurs at lower potentials after Pt and Ru doping (Fig. 3B). These results are clear evidences of the electrocatalytic effect produced by Pt and Ru on the OER.

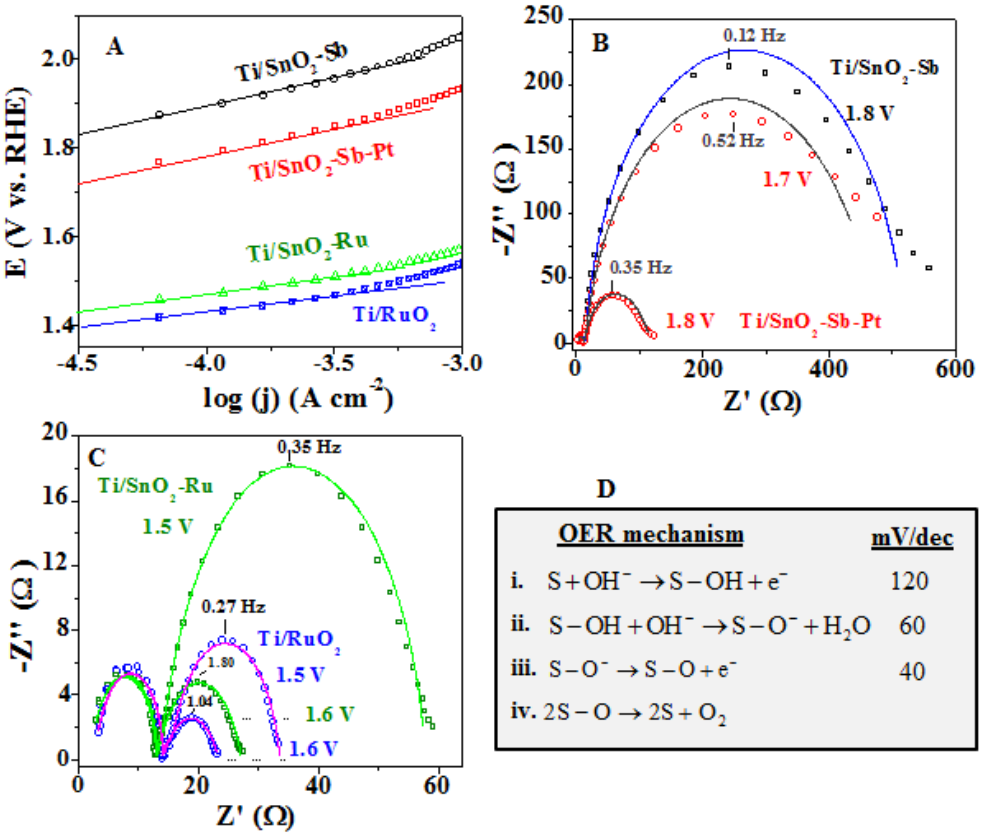

Figure 4. Linear region of Tafel plots for the OER (A) and the complex-plane impedance (Nyquist) plots (B,C) for the different electrodes at different potentials within the OER range: real data (scatter points) and fitted data (solid lines). Electrolyte = 0.1 M NaOH solution. (D) Krasil´shchikov´s mechanism of the OER.

Second, the reaction activity and kinetics of the OER on the studied electrodes were also investigated by Tafel measurements. Figure 4A depicts the Tafel plots of the different electrodes. It is shown that the addition of a small amount of Pt in the SnO_2-based coating lowers the potential values at constant current density, thus increasing its electrocatalytic activity towards the OER. Furthermore, the replacement of Sb by Ru causes a much more marked decrease in these potentials, approaching the behavior of the Ti/RuO_2 electrode. Similar catalytic effects of Ru on the OER were observed by other authors in acidic medium [42,51,59].

Figure 4A also shows that all the plots exhibit a linear region at moderate current densities where the Tafel law is valid [43,48,60]. The operational form of the Tafel equation establishes a linear relationship between the electrode potential and log j, from which the Tafel slope, b (V/dec), and the y-intercept at log j=0, a (V), can be readily extracted. This latter parameter is related to the exchange current density, j_0 (A/m^2), as follows:

$$a = E_{eq} - b \log j_0 \qquad (2)$$

where E_{eq} is the equilibrium potential (V). According to eq(2), the higher the exchange current density, the lower *a*. When expressed in the RHE scale, the equilibrium potential can be set to the standard potential of the reaction ($E^0_{OER} = 1.23\ V$) to a very good approximation, because evolving water-saturated oxygen practically behaves as an ideal gas at room temperature and atmospheric pressure.

The calculated *a* constants and their derived j_0 are collected in Table 2. In general, these values lie in the order of those reported in the literature for similar electrodes [36,39,51]. The results indicate that the *a* parameter of the Ti/SnO_2-Sb anode is reduced by Pt doping and, to a much greater extent, by the replacement of Sb by Ru, involving a considerable acceleration (increase in j_0) of the OER kinetics. Interestingly, the OER rate on Ti/SnO_2-Ru anodes approaches that on the Ti/RuO_2 one.

Third, the activity of the electrodes towards the OER was also analyzed by EIS. Figures 4B and 4C compare the EIS spectra of the different electrodes at potentials close to the OER. At these potentials, the so-called *overpotential region*, a new semicircle associated to the OER is observed. The diameter of this semicircle relates to the Faradaic resistance of the OER ($R_{OER,\eta}$) at a given overpotential (η). The values of $R_{OER,\eta}$ of the different electrodes were calculated at different potentials by fitting the experimental EIS spectra with the corresponding equivalent circuits (see Fig. S5 in the SI). Figures 4B and 4C contain both the experimental (scatter points) and simulated (solid lines) data. As it can be observed, the agreement between experimental and simulated data for the Ru-containing electrodes is quite good in the whole range of tested frequencies (Fig. 4C). However, for the Ti/SnO_2-Sb and the Ti/SnO_2-Sb-Pt electrodes, the semicircles distort at the lowest frequencies and simulated data slightly differ from the experimental one (Fig. 4B). This deviation could be due to some diffusion problem of O_2 or any other phenomena related to the more *non-active* nature of these electrodes.

Table 2. Effect of the anode on the Tafel slopes (a), Tafel line y-intercepts (b) and the charge transfer resistances for the OER ($R_{OER,\eta}$) in 0.1 M NaOH, at different potentials, calculated from polarization curves and EIS data, respectively.

			Electrode			
		Potential (V vs. RHE)	Ti/**SnO_2-Sb**	Ti/**SnO_2-Sb-Pt**	Ti/**SnO_2-Ru**	Ti/**RuO_2**
EIS	**$R_{OER,\eta}$ (Ω)**	**1.4**	---	---	1446	418
		1.5	---	7472	42	18
		1.6	231000	1738	14	10
		1.7	23530	462	---	---
		1.8	474	100	---	---
Tafel	**b (mV dec^{-1})**		124	119	66	56
	a (V vs. RHE)		2.39	2.27	1.74	1.66
	j_0 (A/cm^2)		$4.59x10^{-10}$	$1.82x10^{-9}$	$2.08x10^{-8}$	$2.44x10^{-8}$

The $R_{OER,\eta}$ values of the different electrodes at different potentials are collected in Table 2. In general, the value of R_{OER} is expected to decrease with the increase in the electrode potential [52]. Because the AC signal applied to the electrode/solution interface is small, the OER charge-transfer resistance can be viewed as a dynamic or differential resistance, i.e. the partial derivative of electrode potential over current density. Therefore, whenever the anodic Tafel approach is valid, a drop in $R_{OER,\eta}$ with the increasing overvoltage is predicted [48,61]. Owing to its reciprocal relation to the exchange current density [48], the value of the $R_{OER,\eta}$ at a given electrode potential can be also taken as a measurement of the kinetics of the reaction at such potential: the lower the R_{OER}, the higher j_0, i.e., the kinetic reversibility of the reaction.

Table 2 shows that the Ti/SnO_2-Sb electrode presents remarkably much higher $R_{OER,\eta}$ values than the other electrodes, highlighting its poorer electrocatalytic activity for the OER and its potential for the electrochemical mineralization of organic pollutants. On the contrary, the Ti/RuO_2 electrode shows the lowest $R_{OER,\eta}$ values at any electrode potential, stressing its good electrocatalytic properties for the OER. Interestingly, the $R_{OER,\eta}$ for the Ti/SnO_2-Sb electrode at 1.8 V is even higher than that of the Ti/RuO_2 electrode at 1.4 V. On the other hand, the introduction of small amounts of Pt or Ru in the SnO_2 coating produces a huge decrease in the $R_{OER,\eta}$ values, involving a remarkably electrocatalytic effect on the OER. In particular, at 1.6 V

the Pt(3%) and Ru(13%) dopants reduce the $R_{OER,\eta}$ values by more than two and four orders of magnitude, respectively.

Finally, the OER mechanism on the studied electrodes has been analyzed. The Tafel slope (*b*) reflects the conditions of adsorption of reaction intermediates, so a change in Tafel slope entails a change in reaction mechanism or in the rate determining step [48,51]. Particularly, it is generally accepted that the OER on oxide electrodes and alkaline medium follows the Krasil´shchikov´s mechanism [43]. This mechanism considers that the catalytic activity and the rate determining step for a certain oxide material depends on the interaction strength of the metal oxide and the oxygenated intermediates [51].

The reaction steps and corresponding theoretical Tafel slopes (according to the Krasil´shchikov´s mechanism) are included in Figure 4D, whereas the calculated Tafel slopes are compiled in Table 2. As it can be seen, in 0.1 M NaOH the Tafel slopes for the studied Ti/SnO_2-Sb and Ti/SnO_2-Sb-Pt electrodes are close to 120 mV dec^{-1}. This high Tafel slope indicates that the OER is kinetically controlled by the oxidative adsorption of hydroxyl anions (see eq. (i) in Fig. 4D) and reflects the depressed electrocatalytic activity of SnO_2-based anodes towards the OER [36,51] when compared with Ru-containing metal oxides (see below). From this result it can be inferred that Pt doping does not affect significantly the OER mechanism. However, the observed increase in $j_{0,}$ together with the electrocatalytic effect of Pt on the OER observed by CV and EIS techniques, suggests that it may enhance the intrinsic ability of the solid surface to catalyze the reaction. This effect might be attributed to a favored interaction of Pt with $^{-}$OH and/or $^{\bullet}$OH species, which may somehow promote the OER.

By contrast, the reaction mechanism is greatly affected in the case of Ti/SnO_2-Ru electrode. The Tafel slope below 60 mV dec^{-1} observed for the Ti/RuO_2 electrode agrees with the behavior of this type of anodes [16,49,62] and may involve the electrooxidation of the intermediate surface complex as the rate-determining step (see eq. (iii) in Fig. 4D). When Sb is replaced by Ru in the Ti/SnO_2-Sb electrode, the Tafel slope decreases from 124 mV dec^{-1} to 66 mV dec^{-1}, probably indicating the formation of S−O^{-} surface intermediate as the rate-determining step (see eq. (ii) in Fig. 4D). This variation of Tafel slope suggests a weakening of the metal-oxygen bond and, consequently, a faster discharge of the initial $^{-}$OH ion with surface oxidation. This can be reasonably explained by considering that the substitution of Sb, which is an electronic semiconductor with no marked redox behavior in the studied potential range, by Ru into the SnO_2-Sb phase introduces a higher redox activity, a carrier transport mechanism change and an

increase in its electrical conductivity [39,51]. Both the modification of the reaction mechanism and the increase in j_0 reflect an outstanding electrocatalytic effect of Ru on the OER over Ti/SnO_2-based electrodes.

3.5. Phenol electro-oxidation

Figure 5 shows the voltammetric cycles of the different electrodes in a 0.1 M NaOH and 1000 mg/l phenol solution. For comparison purposes, the steady voltammogram of each electrode in the supporting electrolyte in the absence of phenol is also presented. During the first scan towards positive potentials, the voltammetric profile of the Ti/SnO_2-Sb electrode (Fig. 5A) is unaffected by the presence of phenol until ca. 1.4 V and then, the anodic current sharply increases because of phenol oxidation. In the reverse scan, the oxidation current remains even higher than that of the forward scan between 1.45 to 1.65 V, highlighting the extent of oxidation in this electrode. In the case of the electrode with Pt (Fig. 5B), a small anodic current rises from 0.9 V to 1.30 V in the presence of phenol and then, the onset of phenol electro-oxidation shifts 0.1 V to lower potentials respect to the electrode without Pt. This potential shift seems to point out an electrocatalytic effect of Pt in the response of Ti/SnO_2-Sb electrodes towards the phenol electro-oxidation.

During the reverse scan towards less positive potentials, the cathodic current does not show any related reduction counterpart, reflecting the irreversibility of phenol electro-oxidation reaction in these electrodes (Fig. 5A and 5B). However, an increase in the cathodic current can be observed at 1.0 V for the Ti/SnO_2-Sb anode, giving rise to redox processes centered at 0.91 and 0.66 V (Fig. 5A). These processes could be related to the reduction of some products formed during the previous phenol oxidation. In the case of the Ti/SnO_2-Sb-Pt electrode this reduction current seems to be coupled to the reduction peak of Pt oxides (C_1) centered at 0.6 V and only the first reduction process is discerned.

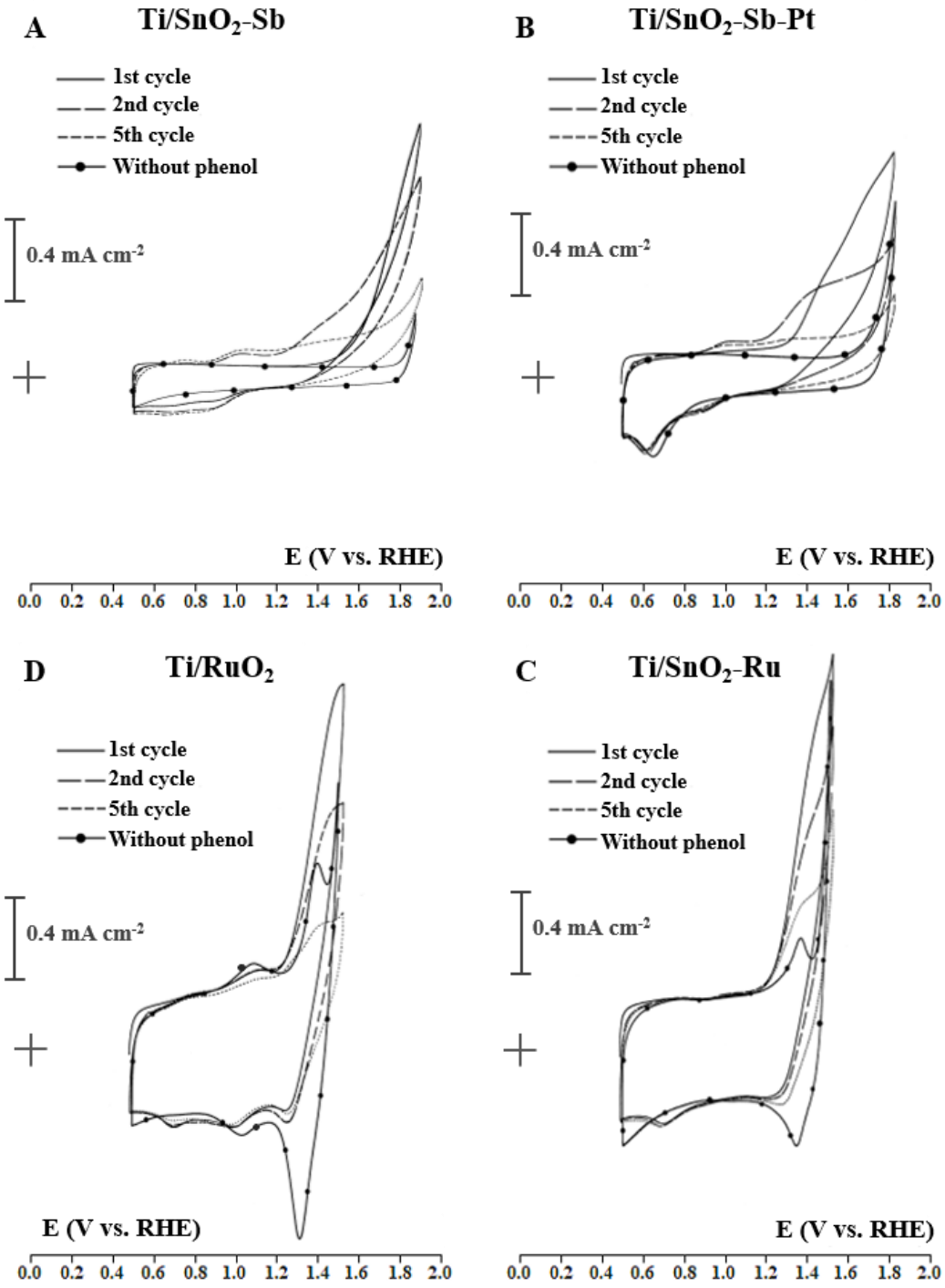

Figure 5. Successive 1st, 2nd and 5th cyclic voltammograms of the (A) Ti/SnO_2-Sb; (B) Ti/SnO_2-Sb-Pt; (C) Ti/RuO_2 and (D) Ti/SnO_2-Ru electrodes in a 0.1 M NaOH + 1000 mg/l de phenol solution. v= 20 mV s^{-1}.

In the second anodic scan, both anodes show two oxidation peaks at 0.74 and 1.01 V, which are attributed to the electrochemical oxidation of any by-product produced after the first voltammetric scan. Afterwards, the anodic current increases again from 1.20 V, showing a broad

oxidation current related to a new oxidation process. This process could be assigned again to the oxidation of any byproduct and/or any process occurring at the modified electrode surface created after the first scan, such as the oxidation of this modified surface or the phenol electro-oxidation at or through this modified surface. During the course of progressive cycling towards higher positive potentials, both electrodes display a gradual decrease in the current density associated to phenol electro-oxidation, thus indicating a progressive deactivation of the electrode for this process [32,63,64]. This surface fouling is related to the formation/deposition of passivating films of oligomeric or polymeric nature [63-65]. In addition, the pairs of reduction and oxidation processes develop to reach a maximum current.

Table 3 lists the potential (E_p) and current density (j_p) of the main phenol electro-oxidation peak at the first scan and the percentage of decreased current density ($\%j_p(i)$ = deactivation percentage) at a given cycle *(i)*. Despite the minute amount of Pt loading, both Figure 5A-B and Table 3 point out some relevant differences between undoped and doped Ti/SnO_2-Sb electrodes: in the presence of Pt (i) both the onset and the course of the phenol electro-oxidation process occur at significantly lower potentials, so that Pt produces an obvious electrocatalytic effect on phenol oxidation; (ii) the charge associated to this oxidation process (in the first forward scan) increases, though the maximum oxidation current (j_p) decreases; and (iii) the deactivation percentage during cycling remarkably increases, so suggesting that such dopant may favor surface fouling. In particular, in the absence of Pt, the passivation of the electrode increases from 26 % to 77% within the first 5 cycles, and up to 86 % in the 10th cycle. This cycling deactivation is considerably slower than in the presence of Pt, which causes a higher passivation in 5 cycles (94 %) than the Ti/SnO_2-Sb electrode in 10 cycles (86 %).

Table 3. Effect of the anode on the peak position (E_p) of phenol oxidation, the current density at this position (j_p) (after double-layer correction) and the electrode passivation ($\%j_p(i)$) during the 2nd, 5th and 10th cycles, in 0.1 M NaOH + 1000 mg L^{-1} phenol. v = 20 mV s^{-1}.

Electrode	**E_p (V)**	**j_p (mA cm^{-2})**	**% $j_{p(2)}$**	**% $j_{p(5)}$**	**% $j_{p(10)}$**
Ti/SnO_2-Sb	1.79	0.90	26	77	86
Ti/SnO_2-Sb-Pt	1.66	0.87	45	94	100
Ti/SnO_2-Ru	1.46	1.48	36	67	80
Ti/RuO_2	1.52	1.61	43	85	96

Figure 5C presents the successive cyclic voltammograms obtained for the Ti/RuO_2 electrode in NaOH + 1000 mg/l of phenol. During the first scan towards positive potentials, a decrease in the current related to the Ru(IV) → Ru(VI) redox transition (A'_3) is observed and next, the anodic current sharply raises at 1.1 - 1.2 V due to phenol oxidation. In this case, the phenol oxidation process is located just in the potential range where the redox transition A'_4 is observed. During the opposite scan, a strong decrease in the cathodic current related to the counterpart C'_4 redox transition (between 1.4-1.2 V) is observed. During the subsequent cycles, the anodic current associated to the phenol electroxidation process progressively decreases up to 96 % (within the first 10^{th} cycles) as a consequence of the electrode passivation. In this case, the blockage is higher than that of the Ti/SnO_2-Sb electrode (mainly during the second cycle), but much lower than in the case of the electrode doped with Pt.

The effect of Ru on the response of SnO_2 towards phenol oxidation is shown in Fig. 5D and Table 3. The introduction of Ru in the oxide shifts the phenol oxidation to lower positive potentials than those of the Ti/SnO_2-Sb electrode, producing a electrocatalytic effect similar to that of Pt doping. However, in this case the oxidation of phenol is located, as in the case of the Ti/RuO_2 electrode, in the region of Ru(VI) to Ru(VII/VIII) redox transition (A'_4) and a marked depression of the reduction counterpart (C'_4) is observed in the subsequent reverse scan. On the other hand, Table 3 also shows that the effect of Ru on the deactivation process is more important during the first cycles but in general much less marked than that of Pt in the Ti/SnO_2-Sb electrode.

Finally, the effect of the phenol concentration (200-1000 ppm) on the voltammetric response of the different electrodes was studied (see Fig. S6 in Supp. Info). For a fixed electrode potential prior to the OER, the oxidation current density on Ti/SnO_2-Sb linearly increased with the phenol concentration, whereas it did not follow an obvious proportional trend for Ti/RuO_2 and Ti/SnO_2-Ru (Fig. S7). In the case of Ti/SnO_2-Sb-Pt, the increase in oxidation current was asymptotic. On the other hand, the onset potential for phenol electro-oxidation on Ti/SnO_2-Sb, Ti/RuO_2 and Ti/SnO_2-Ru electrodes was found to be practically independent of the phenol concentration, while it clearly shifted to less positive potentials with the phenol concentration for Ti/SnO_2-Sb-Pt (Fig. S6).

The use of cyclic voltammetry to study the electro-oxidation and/or electropolymerization of phenol on various metals is extensive in the literature. However, few works deal with the cycling response of MOx electrodes in the presence of phenol. Respect to the Ti/SnO_2-Sb-Pt anode, it

can be inferred that the extent of its deactivation (Table 3) is considerably lower than with (pure) metallic Pt, which showed deactivations above 90 % in the 2nd cycle at even lower phenol concentrations under several electrolyte conditions [63-65]. Nevertheless, the comparison with a previous work [32] suggests a marked influence of the electrolyte and/or pH in the Pt passivating effect on SnO_2-based electrodes. Thus, whereas Pt is proved to promote electrode passivation upon cycling in NaOH (Table 3), in 0.5 M H_2SO_4 electrolyte the deactivation of the 13 at. % Pt electrode (% $j_{p(5)}$ ca. 22 %) was considerably lower than that shown by the Ti/SnO_2-Sb electrode (% $j_{p(5)}$ ca. 48 %). On the other hand, very little information can be found on the cycling response of RuO_2 and/or Ru-doped MOx anodes. The study of a RuO_2(40 atom %)–TiO_2(60 atom %)/Ti electrode showed a ca. 66 % deactivation after the first 5 cycles in a 0.5 M H_2SO_4 solution [66], which is in the order of the studied Ti/SnO_2-Ru in NaOH (Table 3).

3.5.1. Phenol electro-oxidation mechanism on Ru- and Pt-doped SnO_2-based anodes

The mechanism of phenol electro-oxidation has been previously studied by several authors [28,30,67,68]. It is generally accepted that on most electrodes, even on metals, this mechanism implies the formation and/or participation of an oxidized surface monolayer. According to Comninellis et al. [5], on metallic-oxide electrodes the reaction pathways of the electro-oxidation of organic compounds and the OER are closely related, since both involve the adsorption of hydroxyl radicals ($^{\bullet}OH$) after the electrochemical oxidation of water (or ^{-}OH) molecules on the electrode surface. Then, two different behaviors can be distinguished depending on the nature and redox properties of the metal ions in the oxide.

On the one hand, in *non-active* oxides the metal ion cannot increase its oxidation state above the thermodynamic potential for the OER (1.23 V vs. SHE) [2,5]. Consequently, it cannot accommodate more oxygen atoms to form a higher oxide, and it weakly interacts with the hydroxyl radicals. Thus, the electro-oxidation of organics and/or the competing OER are non-specifically mediated by these "physisorbed" hydroxyl radicals. On the other hand, in *active* oxides the metal ion can exhibit higher oxidation states to form a stronger interaction with the hydroxyl radical ($^{\bullet}OH$) and, thus, the so-called higher oxide (MO_{x+1}) acts as a mediator in the oxidation of organics or chemically decompose to evolve O_2 as competitive side reaction.

The sharp rise in the anodic current observed for the Ti/SnO_2-Sb electrode (Figure 5A), occurring at high potentials close to or together with the OER (above 1.4 V), and without previous specific processes (i.e. anodic currents), clearly reflects the *non-active* nature of this

anode. The absence of effects of phenol concentration on the onset potential for phenol electro-oxidation (Fig. S6) is in line with this behavior. Thus, this electrode neither participate in the electro-oxidation reaction nor provide any catalytic active site for the adsorption of reactants and/or products in the aqueous medium. On the other hand, although the observed linear trend between electro-oxidation current and [PhOH] (Fig. S7) was suggested to be an experimental evidence of "direct" (non-mediated) oxidation prior OER [8], Kapałka et al. demonstrated that the presence of organics shifts the I–V curves of *non-active* anodes towards lower potentials. This was assigned to a faster reaction rate between organics and •OH [12]. Thus, all the obtained results support the *non-active* behavior of this anode.

By contrast, in the case of Ti/RuO_2, the electro-oxidation of phenol occurs, just before the OER (Figure 5C), in the potential range of one of the surface redox couples of the metal ion (A'_4), which may actively participate in the reaction. This electrochemical response is characteristic of *active* oxides and has been previously observed by other authors on both pure RuO_2 [69] and mixed Ru oxides [41,66,69,70]. According to these authors, the decrease in the cathodic current during the reverse scan (C'_4) suggests that phenol and/or some of its oxidation products are indirectly oxidized by the highest oxidized Ru species (VII [69] and/or VIII [70]) which are electrochemically generated during the first forward voltammetric scan. Therefore, phenol electro-oxidation is proposed to occur through an electrochemical-chemical mechanism:

$$Ru(VI) \rightarrow Ru(VII)/Ru(VIII) + n\,e^- \quad (3)$$

$$(chemical\ step) \qquad Ru(VII)/Ru(VIII) + PhOH/Product \rightarrow Product' + Ru(VI) \quad (4)$$

the global process being:

$$PhOH/Product \rightarrow Product' + n\,e^- \quad (5)$$

Similarly, the obtained results show that the higher electrocatalytic activity of Ti/SnO_2-Ru electrodes towards phenol oxidation (Figure 5D) is ascribed to the mediation of Ru ions with higher oxidation states (electronic factors). Such a participation of Ru species may occur via highly reversible surface redox reactions somehow like those of equations 3-4. Therefore, by Ru doping, the Ti/SnO_2-Ru electrode behaves like an *active* material. This supremacy of electronic factors on binary Sn-Ru mixed metal oxides is in agreement with previous studies in acid medium [51]. Finally, the non-linear increase in the oxidation current with the phenol

concentration on Ti/RuO_2 and Ti/SnO_2-Ru is in line with a mediated oxidation process [8] and their *active* character.

The introduction of Pt into Ti/SnO_2-Sb anodes also results in an electrocatalytic effect towards phenol oxidation (Figure 5B). In this case, no depression of the reduction counterpart (C_1) is observed in the reverse scan, even though the phenol oxidation occurs across the electrode potentials of A_1. This result suggests that the redox participation of PtOx in the oxidation reaction (like in the example of eq. 4) may be hindered. This finding is reasonably supported by the irreversibility of the Pt/PtOx transitions and the unavailability of higher Pt oxidation states above Pt(IV). Hence, the electrocatalytic effect assigned to Pt may arise from different reasons. In order to explain it, the discussion is focused on the current rise observed between 0.9 V to 1.30 V in the first positive scan (Figure 5B). This is assigned to a strong specific adsorption of phenol (phenolate) on Pt or PtOx active sites [63]. In fact, this adsorption must be electrostatically favored in alkaline conditions because of the molecule deprotonation. This is supported by the fact that such an adsorption-related process was not observed over the Ti/SnO_2-Sb-Pt electrodes in acid medium [32]. Hence, the observed strong interaction Pt/PtOx-phenol at the electrode surface is proposed to facilitate its reaction with the hydroxyl radicals and, therefore, catalyze the phenol oxidation reaction. The much greater deactivation percentage of the electrodes caused by Pt in alkaline conditions (Table 3), the increase in the oxidation current with the phenol concentration (Fig. S7) and the observed shift of the electro-oxidation onset (to less-positive potentials) by increasing the phenol concentration (Fig. S6) strengthen this hypothesis.

In the case of Pt-doped Ti/SnO_2-Sb anodes in acid medium, it has been reported that the activity towards the OER was controlled by the Pt loading (governed by electronic factors) [36], and the higher PhOH oxidation efficiency of the Ti/SnO_2-Sb-Pt(3%) electrode under galvanostatic conditions was assigned to geometric factors (higher compactness) prevailing over electronic ones [32]. However, the specific Pt/PtOx-phenol interaction was not considered. Nevertheless, if it plays a relevant role, this interaction would be an electronic factor (caused by the Pt dopant) that, unlike the case of the competing OER, would favor the phenol oxidation. Accordingly, the Pt/PtOx-phenol interaction proposed in the present work could support or better explain why the Ti/SnO_2-Sb-Pt(3%) electrode showed better phenol oxidation efficiency than Ti/SnO_2-Sb also in acid medium.

In this work, the calculated voltammetric oxidation charge due to phenol oxidation (measured within the first voltammetric scan and normalized by the roughness factor, *Rf* at 0.55 V in Table 1) on the Ti/SnO_2-Sb anode increases from 0.0264 mC/cm^2 (real area) to 0.0319 mC/cm^2 and 0.0288 mC/cm^2 (real area) by Pt and Ru doping, respectively. Hence, and although the secondary factors may also affect, the obtained results clearly reveal that in alkaline conditions the electronic factors govern the electrochemical response of these electrodes. In fact, under alkaline conditions the specific adsorption of phenolate and hydroxyl ions on the Pt surface (positively polarized) must be favored compared to that of the corresponding protonated species in acidic media. This specific interaction of the doping metal is, then, so important that it can determine the electrocatalytic behavior of the electrode and/or it can lead to controversial results if not considered.

From all these results, the participation of metallic species via the specific adsorption of the organic molecules is proposed to be considered in the generalized scheme of the electrochemical conversion/combustion of organics with simultaneous OER on mixed oxide electrodes, as exemplified for the studied SnO_2-based electrodes in Figure 6. This scheme summarizes the observed *active* behavior of the Ru-doped SnO_2 mixed oxides forming $(Ru_\delta Sn_{1-\delta})O_2$ solid solutions (green route in Figure 6) and the "*non-redox active*" behavior of Pt-doped SnO_2 mixed oxides, in which the segregated metallic Pt/PtOx species favor (participate in) the reaction by specific interactions, without reversible redox reactions (orange route in Fig. 6). Nevertheless, the pure *non-active* behavior should not be ruled out (blue route in Fig. 6), since it may also occur on some Sn atoms. Since the Pt/PtOx particles are intimately embedded by the SnO_2-Sb phase (see Fig. 1), it seems reasonable that the highly oxidizing hydroxyl radicals formed on the *non-active* SnO_2-Sb phase may be able to react with the adsorbed phenol on Pt/PtOx. This synergetic effect may explain the better electrocatalytic performance of Ti/SnO_2-Sb-Pt(3%) anode towards phenol oxidation.

The participation of specific interactions in the electro-oxidation of pollutants over M'MOx anodes agrees with other results in the literature [71,72], but it has been demonstrated (experimentally supported) in few cases. For example, we used in-situ SERS to demonstrate that the specific adsorption of CN^- on lattice Cu^{2+} atoms remarkably enhances the electrocatalytic activity of $Cu_xCo_{3-x}O_4$ spinels towards the electro-oxidation of this pollutant [72]. In this case, both Co and Cu can participate with reversible redox couples in the oxidation of CN^-, so the behavior of the mixed metal oxide is considered *active* with proved interactions. Accordingly,

the different mixed metal oxides may involve distinct catalytic pathways that must be studied and considered to complete a more complex scheme of the electrochemical conversion/combustion of organics with simultaneous OER in these materials.

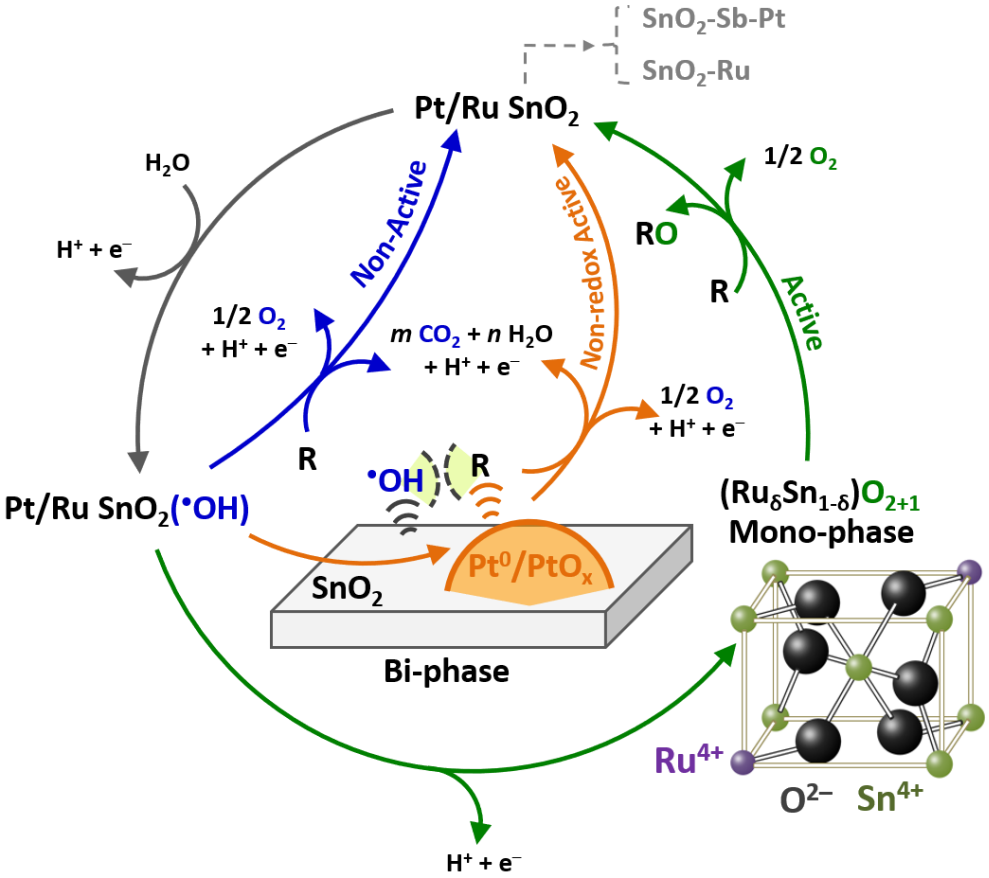

Figure 6. Scheme of the electrochemical conversion/combustion of organics with simultaneous OER on Pt/Ru doped SnO_2 mixed oxide electrodes, as adapted from [5].

On the other hand, we have recently demonstrated that, unlike Cu, Au segregates in the form of particles in cobalt spinels and that it does not catalyze the CN^- electro-oxidation [73]. This has been assigned to a too-strong adsorption of cyanide and/or to its inaccessibility to chemisorbed hydroxyl radicals on Co_3O_4 phase. In Ti/SnO_2-Sb anodes, the loss in phenol degradation performance when the Pt loading was increased from 3 at. % to 13 at. % [32] could be also partly related to a less efficient pollutant-(•OH) interaction caused by an increase in the size of Pt-enriched segregated phase. Nevertheless, the parallel enhancement on the OER performance with the Pt loading may be the predominant effect. Hence, not only the nature but also the segregation and dimensions of dopant phases may play a key role on these catalytic pathways. All these

results stress the significance of the anode design on the control and optimization of their catalytic properties.

4. Conclusions

The present work analyzes the role of Ru and Pt dopants on the electrocatalytic behavior of Ti/SnO_2-Sb anodes under alkaline conditions. The obtained results show that the introduction of a small amount of Pt and the replacement of Sb by Ru in the Ti/SnO_2-Sb electrode produce marked changes on its electrochemical response in NaOH medium. Both species introduce their characteristic but different solid-state redox processes: while the Pt/PtOx redox process is quite irreversible and spread out over a wide range of electrode potentials, ruthenium involves various and highly reversible redox processes.

The different characterization techniques indicate that both dopants decrease the onset potential, the potential at constant current density and the charge-transfer resistance of Ti/SnO_2-Sb anodes for the OER, thus, causing a significant electrocatalytic effect towards this reaction in this electrolyte. However, Tafel measurements reveal an outstanding difference between these species: while Pt mainly affects the kinetics (j_0) of the OER, Ru modifies the rate-determining step (the mechanism). Interestingly, the quite similar capacitance behavior (geometric factors) of the studied Ti/SnO_2-based anodes, found by cyclic voltammetry and EIS, demonstrates that their different electrocatalytic responses can be unambiguously assigned to the nature of their different components, i.e. true electrocatalytic effects (electronic factors).

Finally, the shift of phenol oxidation towards lower positive potentials observed by voltammetry permits to conclude that the capability of Ti/SnO_2-Sb anodes towards this reaction in alkaline medium is also enhanced by Pt and Ru dopants. In addition, the voltammetric study suggests that both Pt and Ru dopants seem to participate in the reaction, thus, introducing certain *active* character to the *non-active*·SnO_2-Sb mixed oxide. The electrocatalytic effect of Pt is associated to a strong specific adsorption of phenol on Pt/PtOx sites, without participation of the irreversible Pt/PtOx couple ("*non-redox active*" behavior). On the contrary, the higher oxidation states of Ru species actively and reversibly mediate in the oxidation process. Hence, the different redox features of the dopants strongly affect and must be considered to elucidating the nature and electrocatalytic behavior of SnO_2-based oxides.

Acknowledgements

Financial support from the Spanish Ministerio de Economía y Competitividad and FEDER funds (MAT2016-76595-R, IJCI-2014-20012) and Generalitat Valenciana (PROMETEO/2018/087) are gratefully acknowledged.

References

[1] K. Rajeshwar, J.G. Ibanez, Environmental Electrochemistry: Fundamentals and Applications in Pollution Abatement, Academic Press Inc., San Diego (1997).

[2] C.A. Martínez-Huitle, S. Ferro, Electrochemical oxidation of organic pollutants for the wastewater treatment: direct and indirect processes, Chem. Soc. Rev. 25 (2006) 1324–1340.

[3] E. Brillas, C.A. Martínez-Huitle, Decontamination of wastewaters containing synthetic organic dyes by electrochemical methods. An updated review, Appl. Catal. B: Environ. 166-167 (2015) 603-643.

[4] M. Panizza, G. Cerisola, Direct And Mediated Anodic Oxidation of Organic Pollutants, Chem. Rev. 109 (2009) 6541-6569.

[5] Ch. Comninellis, Electrocatalysis in the electrochemical conversion/combustion of organic pollutants for waste water treatment, Electrochim. Acta 39 (1994) 1857-1862.

[6] C.A. Martínez-Huitle, S. Ferro, A. De Battisti, Electrochemical Incineration in the Presence of Halides, Electrochem. Solid-State Lett. 8 (2005) D35-D39.

[7] O. Scialdone, A. Galia, C. Guarisco, S. Randazzo, G. Filardo, Electrochemical incineration of oxalic acid at boron doped diamond anodes: Role of operative parameters, Electrochim. Acta 53 (2008) 2095-2108.

[8] O. Scialdone, S. Randazzo, A. Galia, G. Filardo, Electrochemical oxidation of organics at metal oxide electrodes: The incineration of oxalic acid at IrO_2–$Ta2O_5$ (DSA-O_2) anode, Electrochim. Acta 54 (2009) 1210-1217.

[9] O. Scialdone Electrochemical oxidation of organic pollutants in water at metal oxide electrodes: A simple theoretical model including direct and indirect oxidation processes at the anodic surface, Electrochim. Acta 54 (2009) 6140-6147.

[10] A. Kapałka, B. Lanova, H. Baltruschat, G. Fóti, Ch. Comninellis, Electrochemically induced mineralization of organics by molecular oxygen on boron-doped diamond electrode, Electrochem. Commun. 10 (2008) 1215-1218.

[11] A. Kapałka, G. Fóti, Ch. Comninellis, Kinetic modelling of the electrochemical mineralization of organic pollutants for wastewater treatment, J. Appl. Electrochem. 38 (2008) 7-16.

[12] A. Kapałka, G. Fóti, Ch. Comninellis, The importance of electrode material in environmental electrochemistry. Formation and reactivity of free hydroxyl radicals on boron-doped diamond electrodes, Electrochim. Acta 54 (2009) 2018-2023

[13] A. Kapałka, H. Baltruschat, Ch. Comninellis, Electrochemical Oxidation of Organic Compounds Induced by Electro-Generated Free Hydroxyl Radicals on BDD Electrodes, in Synthetic Diamond Films: Preparation, Electrochemistry, Characterization, and Applications, E. Brillas, C. A. Martínez-Huitle Eds., John Wiley & Sons, Inc. 2011

[14] C.A. Martínez-Huitle, M. A. Quiroz, Ch. Comninellis, S. Ferro, A. De Battisti, Electrochemical incineration of chloranilic acid using Ti/IrO_2, Pb/PbO_2 and Si/BDD electrodes Electrochim. Acta 50 (2004) 949-956.

[15] O. Scialdone, S. Randazzo, A. Galia, G. Silvestri, Electrochemical oxidation of organics in water: Role of operative parameters in the absence and in the presence of NaCl, Water Res. 43 (2009) 2260-2272.

[16] S. Trasatti (Ed.), Studies in Physical and Theoretical Chemistry. Vol. 11. Electrodes of Conductive Metallic oxides. Part. A-B, Elsevier Science Publishers, Amsterdam (1980/1981).

[17] S. Trasatti, Electrocatalysis: understanding the success of DSA, Electrochim. Acta 45 (2000) 2377-2385.

[18] Ch. Comninellis, G. Chen (Eds.), Electrochemistry for the Environment, Springer, New York (2010).

[19] M. Panizza, P.A. Michaud, G. Cerisola, Ch. Comninellis, Anodic oxidation of 2-naphtol at boron-doped diamond electrodes. J. Electroanal. Chem. 507(1-2) (2001) 206-214

[20] J. Iniesta, P.A. Michaud, M. Panizza, G. Cerisola, A. Aldaz, Ch. Comninellis, Electrochim. Acta 46 (2001) 3573-3578.

[21] O. Scialdone, C. Guarisco, A. Galia, Oxidation of organics in water in microfluidic electrochemical reactors: Theoretical model and experiments, Electrochim. Acta 58 (2011) 463-473.

[22] A. M. Polcaro, M. Mascia, S. Palmas, A. Vacca, Kinetic Study on the Removal of Organic Pollutants by an Electrochemical Oxidation Process, Ind. Eng. Chem. Res. 41 (2002) 2874-2881.

[23] A.N.S. Rao, V.T. Venkatarangaiah, Metal oxide-coated anodes in wastewater treatment, Environ. Sci. Pollut. Res. 21 (2014) 3197-3217.

[24] W. Wu, Z.-H. Huang, T.-T. Lim, Recent development of mixed metal oxide anodes for electrochemical oxidation of organic pollutants in water. Appl. Catal. A: Gen. 480 (2014) 58-78.

[25] C.A. Martínez-Huitle, S. Ferro, Single and Coupled Electrochemical Processes and Reactors for the Abatement of Organic Water Pollutants: A Critical Review, Chem. Rev. 115 (2015) 13362-13407.

[26] F.C. Moreira, R.A.R. Boaventura, E. Brillas, V.J.P. Vilar, Electrochemical advanced oxidation processes: A review on their application to synthetic and real wastewaters, Appl. Catal. B: Environ. 202 (2017) 217-26.

[27] R. Berenguer, T. Valdés-Solís, A.B. Fuertes, C. Quijada, E. Morallón, Cyanide and Phenol Oxidation on Nanostructured Co_3O_4 Electrodes Prepared by Different Methods, J. Electrochem. Soc. 155 (2008) K110-K115.

[28] Ch. Comninellis, Electrochemical treatment of waste water containing phenol, Trans. IChemE 70 (1992) 219–224.

[29] S. Stucki, R. Kotz, B. Carcer, W. Suter, Electrochemical Waste-Water Treatment using High Overvoltage Anodes. 2. Anode Performance and Applications, J. Appl. Electrochem. 21 (1991) 99-104.

[30] Ch. Comninellis, C. Pulgarin, Electrochemical oxidation of phenol for wastewater treatment using SnO_2 anodes, J. Appl. Electrochem. 23 (1993) 108-112.

[31] J.D. Rodgers, W.J. Jedral, N.J. Bunce, Electrochemical Oxidation of Chlorinated Phenols, Environ. Sci. Technol. 33 (1999) 1453-1457.

[32] F. Montilla, E. Morallón, J.L. Vázquez, Evaluation of the Electrocatalytic Activity of Antimony-Doped Tin Dioxide Anodes Toward the Oxidation of Phenol in Aqueous Solutions, J. Electrochem. Soc. 152 (2005) B421-B427.

[33] B. Correa-LozanoCh. ComninellisA. De Battisti, Service Life of Ti/SnO_2-Sb_2O_5 Anodes, J. Appl. Electrochem. 27 (1997) 970-974.

[34] F. Vicent, E. Morallón, C. Quijada, J.L. Vázquez, A. Aldaz, F. Cases, Characterization and stability of doped SnO_2 anodes, J. Appl. Electrochem. 28 (1998) 607-612.

[35] J.C. Forti, P. Olivi, A.R. de Andrade, Characterisation of DSA®-Type Coatings with Nominal Composition Ti/$Ru_{0.3}Ti_{(0.7-x)}Sn_xO_2$ Prepared Via a Polymeric Precursor, Electrochim. Acta 47 (2001) 913-920.

[36] F. Montilla, E. Morallón, A. De Battisti, J.L. Vázquez, Preparation and Characterization of Antimony-Doped Tin Dioxide Electrodes. Part 1. Electrochemical Characterization, J. Phys. Chem. B 108 (2004) 5036-5043.

[37] R. Berenguer, A. La Rosa-Toro, C. Quijada, E. Morallón, Origin of the Deactivation of Spinel $Cu_xCo_{3-x}O_4$/Ti Anodes Prepared by Thermal Decomposition, J. Phys. Chem. C 112 (2008) 16945-16952.

[38] B. Adams, M. Tian, A. Chen, Design and Electrochemical Study of SnO_2-based Mixed Oxide Electrodes, Electrochim. Acta 54 (2009) 1491-1498.

[39] R. Berenguer, J.M. Sieben, C. Quijada, E. Morallón, Pt- and Ru-Doped SnO_2−Sb Anodes with High Stability in Alkaline Medium, ACS Appl. Mater. Interfaces 6 (2014) 22778-22789.

[40] R. Berenguer, J.M. Sieben, C. Quijada, E. Morallón, Electrocatalytic degradation of phenol on Pt- and Ru-doped Ti/SnO_2-Sb anodes in an alkaline medium, Appl. Catal. B: Environ. 199 (2016) 394-404.

[41] P.D.P. Alves, M. Spagnol, G. Tremiliosi-Filho, A.R. de Andrade, Investigation of the influence of the anode composition of DSA-type electrodes on the electrocatalytic oxidation of phenol in neutral medium, J. Braz. Chem. Soc. 15 (2004) 626–634.

[42] R. Berenguer, C. Quijada, E. Morallón, Electrochemical characterization of SnO_2 electrodes doped with Ru and Pt, Electrochim. Acta 54 (2009) 5230-5238.

[43] A.J. Bard, L.R. Faulkner, Electrochemical Methods, John Wiley& Sons, New York (1980).

[44] F. Montilla, E. Morallón, A. De Battisti, S. Barison, S. Daolio, J.L. Vázquez, Preparation and Characterization of Antimony-Doped Tin Dioxide Electrodes. 3. XPS and SIMS Characterization, J. Phys. Chem. B 2004, 108, 15976-15981.

[45] F. Montilla, E. Morallón, A. De Battisti, A. Benedetti, H. Yamashita, J.L. Vázquez, Preparation and Characterization of Antimony-Doped Tin Dioxide Electrodes. Part 2. XRD and EXAFS Characterization, J. Phys. Chem. B 108 (2004) 5044-5050.

[46] Y. He, H. Li, X. Zou, N. Bai, Y. Cao, Y. Cao, M. Fan, G.-D. Li, Platinum dioxide activated porous SnO_2 microspheres for the detection of trace formaldehyde at low operating temperature, Sensor. Actuat. B-Chem. 244 (2017) 475-481.

[47] A.L. Santos, D. Profeti, P. Olivi, Electrooxidation of methanol on Pt microparticles dispersed on SnO_2 thin films, Electrochim. Acta 50 (2005) 2615-2621.

[48] R.L. Doyle, M.E.G. Lyons. The Oxygen Evolution Reaction: Mechanistic Concepts and Catalyst Design, in Photoelectrochemical Solar Fuel Production: From Basic Principles to Advanced Devices. Sixto Giménez, Juan Bisquert (Edts), Springer, 2016, pp. 41-104.

[49] M.E.G. Lyons, S. Floquet, Mechanism of oxygen reactions at porous oxide electrodes. Part 2 - Oxygen evolution at RuO_2, IrO_2 and $Ir_xRu_{1-x}O_2$ electrodes in aqueous acid and alkaline solution, Phys. Chem. Chem. Phys. 13 (2011) 5314-5335.

[50] D. Rochefort, P. Dabo, D. Guay, P.M.A. Sherwood, XPS Investigations of Thermally Prepared RuO_2 Electrodes in Reductive Conditions, Electrochim. Acta 48 (2003) 4245-4252.

[51] J. Gaudet, A.C. Tavares, S. Trasatti, D. Guay, Physicochemical Characterization of Mixed RuO_2-SnO_2 Solid Solutions, Chem. Mater. 17 (2005) 1570-1579.

[52] B.E. Conway, Electrochemical Supercapacitors: Scientific Fundamentals and Technological Applications, Springer, New York (1999).

[53] J. Ribeiro, A.R.de Andrade, Investigation of the electrical properties, charging process, and passivation of RuO_2–Ta_2O_5 oxide films, J. Electroanal. Chem. 592 (2006) 153-162.

[54] G. Lodi, G. Zucchini, A. De Battisti, E. Sivieri, S. Trasatti, On some debated aspects of the behaviour of RuO_2 film electrodes, Mater. Chem. 3 (1978) 179-188.

[55] A.J. McEvoy, W. Gissler, A ruthenium dioxide-semiconductor Schottky barrier photovoltaic device, J. Appl. Phys. 53 (1982) 1251-1252.

[56] N.L. Wu, J.Y. Hwang, P.Y. Liu, C.Y. Han, S.L. Kuo, K.H. Liao, M.H. Lee, S.Y. Wang, Synthesis and Characterization of Sb-Doped SnO_2 Xerogel Electrochemical Capacitor, J. Electrochem. Soc. 148 (2001) A550−A553.

[57] W. Sugimoto, T. Kizaki, K. Yokoshima, Y. Murakami, Y. Takasu, Evaluation of the Pseudocapacitance in RuO_2 with a RuO_2/GC Thin Film Electrode, Electrochim. Acta 49 (2004) 313-320.

[58] S. Ardizzone, G. Fregonara, S. Trasatti, Inner and Outer Active Surface of RuO_2 Electrodes, Electrochim. Acta 35 (1990) 263-267.

[59] C. Iwakura, K. Sakamoto, Effect of Active Layer Composition on the Service Life of (SnO_2 and RuO_2)-Coated Ti Electrodes in Sulfuric-Acid Solution, J. Electrochem. Soc. 132 (1985) 2420-2423.

[60] J.O.M. Bockris, A.K.N. Reddy, M.E. Gamboa-Aldeco (Eds), Modern Electrochemistry 2A: Fundamentals of Electrodics. 2nd Ed. Kluwer Academic/Plenum Publishers: New York (2000).

[61] R.L. Doyle, M.E.G Lyons, An electrochemical impedance study of the oxygen evolution reaction at hydrous iron oxides in base, Phys. Chem. Chem. Phys. 15 (2013) 5224-5237.

[62] Y. Matsumoto, E. Sato, Electrocatalytic Properties of Transition Metal Oxides for Oxygen Evolution Reaction, Mater. Chem. Phys. 14 (1986) 397-426.

[63] M. Gattrell, D.W. Kirk, A Study of the Oxidation of Phenol at Platinum and Preoxidized Platinum Surfaces, J. Electrochem. Soc. 140 (1993) 1534-1540.

[64] R. Lapuente, F. Cases, P. Garcés, E. Morallón, J.L. Vázquez, A voltammetric and FTIR-ATR study of the electropolymerization of phenol on platinum electrodes in carbonate medium. Influence of sulphide. J. Electroanal. Chem. 451 (1998) 163–171.

[65] R. Lapuente, C. Quijada, F. Huerta, F. Cases, J.L. Vázquez, X-Ray photoelectron Spectroscopy study of the composition of polyphenol films formed on Pt by electropolymerisation of phenol in the presence of sulphide in carbonate medium, Polymer J. 35 (2003) 911-919.

[66] V.V. Panić, A.B. Dekanski, T.R. Vidaković, V.B. Mišković-Stanković, B.Ž. Javanović, B.Ž. Nikolić, Oxidation of phenol on RuO_2–TiO_2/Ti anodes, J. Solid State Electrochem. 9 (2005) 43–54.

[67] Y.J. Feng, X.Y. Li, Electrocatalytic oxidation of phenol on several metal-oxide electrodes in aqueous solutions, Water Res. 37 (2003) 2399-2407.

[68] X.Y. Li, Y.H. Cui, Y.J. Feng, Z.M. Xie, J.D. Gu, Reaction pathways and mechanisms of the electrochemical degradation of phenol on different electrodes. Water Res 39 (2005) 1972-1981.

[69] C.L.P.S. Zanta, A.R. de Andrade, J.F.C. Boodts, Electrochemical behaviour of olefins: oxidation at ruthenium-titanium dioxide and iridium±titanium dioxide coated electrodes, J. Appl. Electrochem. 30 (2000) 467-474.

[70] D.T. Cestarolli, A.R. de Andrade, Electrochemical Oxidation of Phenol at $Ti/Ru_{0.3}Pb_{(0.7-x)}Ti_xO_y$ Electrodes in Aqueous Media, J. Electrochem. Soc. 154 (2007) E25-E30.

[71] B. Wels, D.C. Johnson, Electrocatalysis of anodic oxygen transfer reactions:oxidation of cyanide at electrodeposited copper oxide electrodes in alkalinemedia, J. Electrochem. Soc. 9 (1990) 2785-2791.

[72] R. Berenguer, A. La Rosa-Toro, C. Quijada, E. Morallón, Electrocatalytic oxidation of cyanide on copper-doped cobalt oxide electrodes, Appl. Catal. B: Environ. 207 (2017) 286-296.

[73] R. Berenguer, C. Quijada, A. La Rosa-Toro, E. Morallón, Electro-oxidation of cyanide on active and non-active anodes: designing the electrocatalytic response of cobalt spinels, Sep. Purif. Technol. 208 (2019) 42-50.